Author Manuscript

Title: Feasibility of a supporting salt free non-aqueous redox flow battery utilizing ionic active materials

Authors: Jarrod Milshtein; Sydney Fisher; Tanya Breault, Ph.D.; Levi Thompson, Ph.D.; Fikile Brushett, Ph.D.

This is the author manuscript accepted for publication and has undergone full peer review but has not been through the copyediting, typesetting, pagination and proofreading process, which may lead to differences between this version and the Version of Record.

To be cited as: 10.1002/cssc.201700028

Link to VoR: https://doi.org/10.1002/cssc.201700028

Feasibility of a supporting salt free non-aqueous redox flow battery utilizing ionic active materials

Jarrod D. Milshtein,[§[a,b]] Sydney L. Fisher,[§[a,c]] Tanya M. Breault,[[a,c]] Levi T. Thompson,*[[a,c]] and Fikile R. Brushett*[[a,d]]

Abstract: Non-aqueous redox flow batteries (NAqRFBs) are promising devices for grid-scale energy storage, however, high projected prices could limit commercial prospects. One price reduction route is to minimize or eliminate the expensive supporting salts typically employed in NAqRFBs. We demonstrate the feasibility of a flow cell operating in the absence of supporting salt, utilizing ionic active species. These ionic species possess high conductivities in acetonitrile (12 – 19 mS cm^{-1}), and cycle at 20 mA cm^{-2} with energy efficiencies (> 75%) comparable to state-of-the-art NAqRFBs employing high concentrations of supporting salt. A chemistry-agnostic techno-economic analysis highlights the possible cost savings of minimizing salt content in a NAqRFB. This paper offers the first demonstration of a NAqRFB operating without supporting salt. The associated design principles can guide the development of future active species and could make NAqRFBs competitive with their aqueous counterparts.

Introduction

Redox flow batteries (RFBs) have emerged as attractive devices for grid-scale energy storage due to their decoupled power ratings (reactor area) and energy capacities (tank size), as well as their long lifetimes, location independence, and fast response.[1–3] Widespread use of RFBs could facilitate the introduction of intermittent renewables (e.g. solar and wind) into the existing electrical grid while also providing peak shaving and load leveling capabilities.[4,5] Despite these advantages, high system prices (> \$500 kWh^{-1} in 2014)[6,7] have severely limited the commercial deployment of RFBs. To facilitate integration of a 4 h energy storage system, the United States Department of Energy Office of Electricity Delivery and Energy Reliability set a target price of \$150 kWh^{-1}, including installation and power-conditioning equipment costs.[8,9] Recent techno-economic analyses predicted that both aqueous and non-aqueous (NAq) RFBs could reach this aggressive target by decreasing manufacturing costs, advancing materials performance, and improving cell architecture.[6,10] Although not commercially viable yet, NAqRFBs promise a number of advantages over aqueous systems, including broader electrochemical windows (3 – 4 V),[1,11,12] that could enable higher cell energy densities and aid in the implementation of multi-electron transfer materials.[12] Additionally, a wide range of NAq solvents and supporting salts are available, and rational functionalization of the active species can be used to tailor physicochemical and electrochemical properties,[13] providing multiple pathways for device optimization and price reduction.

Future-state prices for NAq supporting electrolytes (solvent + 1 M salt) are anticipated to be relatively high (~\$5 kg^{-1}), as compared to their aqueous counterparts (~\$0.10 kg^{-1}),[6] so decreasing the costs and / or quantities of both the solvent and supporting salt will be critical.[10] A number of studies have focused on enhancing active species solubility,[14–19] which serves to decrease the total amount of solvent required.[10] The supporting salt, however, especially the fluorinated derivatives typically employed in NAq batteries (e.g., lithium hexafluorophosphate, tetrabutylammonium tetrafluoroborate), will constitute a majority of the future-state supporting electrolyte cost (~\$20 kg^{-1} vs. ~\$2 kg^{-1} for the salt and solvent, respectively).[6] Despite the opportunity for substantial cost savings,[10,20] few studies have focused on minimizing supporting salt content. In a prior report, we described a common-ion exchange NAqRFB design that reduced the required amount of supporting salt by employing similarly charged active species that share a common, counter-ion.[20] Additional cost savings are possible through the use of multi-functional materials, which serve two or more critical roles in the electrolyte (i.e., solvation, charge carrier, redox active).[10] Herein, we combine multi-functional active species with the common-ion exchange configuration to demonstrate a NAqRFB proof-of-concept prototype operating in the limit of no supporting salt.

NAqRFBs utilize supporting salts to enhance electrolyte conductivity and maintain electroneutrality during charge and discharge.[1,2] High salt concentrations, however, can limit the solubility of the active species in the electrolyte solution[20–22] and suppress the conductivity of ion-selective membranes, increasing area-specific resistance (ASR).[23] The need for supporting salt can be eliminated entirely by using similarly charged active species (positive or negative) that remain as ions across all accessible states-of-charge (SOCs). In this scheme, counter-ions that are associated with the redox-active ion provide charge balance, and both the active species and counter-ions contribute to the ionic conductivity of the electrolyte. Figure 1 highlights the charging process for a NAqRFB utilizing cationic active species with no supporting salt, where counter-

[a] Joint Center for Energy Storage Research
USA

[b] J. D. Milshtein[§]
Department of Materials Science and Engineering
Massachusetts Institute of Technology

[c] S. L. Fisher,[§] Dr. T. M. Breault, Prof. L. T. Thompson
Department of Chemical Engineering
University of Michigan
2300 Hayward St, Ann Arbor, MI 48109, USA
E-mail: ltt@umich.edu

[d] Prof. F. R. Brushett
Department of Chemical Engineering
Massachusetts Institute of Technology
77 Massachusetts Ave, Cambridge, MA 02139
E-mail: brushett@mit.edu

[§] These authors contributed equally to this work.

Supporting information for this article is given via a link at the end of the document.

Author Manuscript

This article is protected by copyright. All rights reserved

anions transport from the negative electrolyte (negolyte) to the positive electrolyte (posolyte), maintaining electroneutrality. The same concept can be extended to redox-active anions with counter-cations.

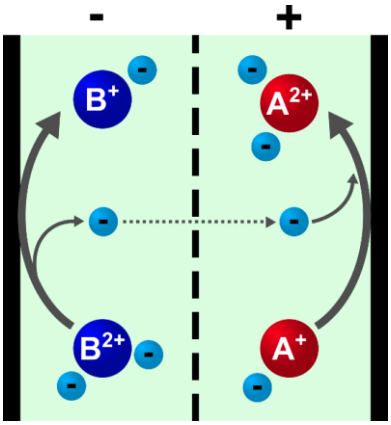

Figure 1. Schematic of the charging process in a supporting salt free RFB employing cationic redox-active species. "A" is the posolyte active material (red), and "B" is the negolyte active material (dark blue). Associating counter-anions are denoted by "-" (light blue).

For this study, we selected iron(II) tris(2,2'-bipyridine) tetrafluoroborate ($Fe(bpy)_3(BF_4)_2$, Figure S1a)[24] and ferrocenylmethyl dimethyl ethyl ammonium tetrafluoroborate ($Fc1N112\text{-}BF_4$, Figure S1b)[15,16] as model ionic redox active species to demonstrate the salt free cell concept. The lack of viable NAqRFB chemistries, especially those with the characteristics necessary for the demonstration of a salt free device, drove our selections. $Fc1N112\text{-}BF_4$ is known to be a highly soluble and stable posolyte active material,[15,16,20] however, it is too expensive for implementation in a low cost grid-scale device.[10] $Fe(bpy)_3(BF_4)_2$ is one of the only well-characterized NAqRFB negolyte active materials that remains as a cation across all relevant SOCs, but suffers from relatively poor stability.[20,24] Both species have been investigated extensively in prior literature, have well-characterized properties, and are therefore excellent model compounds.

In this system, $Fe(bpy)_3^{2+}$ and $Fc1N112^+$ act as the redox-active cations (at 0% SOC), while BF_4^- serves as the common, charge balancing, counter-anion. The posolyte and negolyte half-cell reactions are provided in Equations (1) and (2), respectively, while Equation (3) shows the full-cell reaction:

$$\left[Fc1N112^{2+}\right]\left[BF_4^-\right]_2 + e^- \rightleftharpoons \left[Fc1N112^+\right]\left[BF_4^-\right] + BF_4^- \quad (1)$$

$$\left[Fe(bpy)_3^{2+}\right]\left[BF_4^-\right]_2 + e^- \rightleftharpoons \left[Fe(bpy)_3^+\right]\left[BF_4^-\right] + BF_4^- \quad (2)$$

$$\left[Fe(bpy)_3^{2+}\right]\left[BF_4^-\right]_2 + \left[Fc1N112^+\right]\left[BF_4^-\right] \rightleftharpoons \left[Fe(bpy)_3^+\right]\left[BF_4^-\right] + \left[Fc1N112^{2+}\right]\left[BF_4^-\right]_2 \quad (3)$$

Importantly, these active species are positively charged at all relevant oxidation states, enabling the salt free cell configuration outlined in Figure 1. Additionally, these compounds exhibit minimal inter-species reactions in the singly charged state, are soluble in acetonitrile (MeCN), and are easily synthesized in large quantities, facilitating a proof-of-concept flow cell enlisting the no supporting salt framework.[20]

This study demonstrates a NAqRFB configured to operate in the absence of any supporting salt, utilizing well-studied model active species. First, conductivity measurements demonstrate the high conductivities of the model ionic active species in MeCN. Second, cyclic voltammetry (CV) and bulk electrolysis experiments show that the ionic active species maintain redox activity in the absence of supporting salt. Third, proof-of-concept flow cell experiments demonstrate the feasibility of a supporting salt free NAqRFB, exhibiting resistances and efficiencies similar to those of other recently reported NAqRFBs.[25,26] Finally, a chemistry-agnostic techno-economic analysis highlights the significant cost savings afforded by minimizing or eliminating the amount of salt in NAqRFBs with varying active species costs, salt costs, and cell potentials. Overall, this paper highlights the design of a NAqRFB operating without supporting salt. Further, the design and configuration principles of NAqRFBs employing similarly charged, all-ionic active species outlined in this work can extend beyond the model compounds to other active species, including organic molecules, providing a viable route to minimizing the price of promising future NAqRFBs.

Results and Discussion

Active Species Conductivity

To demonstrate the feasibility of performing electrochemical experiments in solutions of MeCN with no supporting salt, the conductivities of the active species are measured and compared to those of supporting salts typically employed in NAqRFBs. Figure 2 illustrates the high conductivities afforded by 0.2 M of the ionic active species in MeCN, especially in comparison to 0.2 M lithium tetrafluoroborate ($LiBF_4$) and tetraethylammonium tetrafluoroborate ($TEABF_4$) in the same solvent. Not shown in this figure is the conductivity of an equimolar solution containing 0.2 M $Fc1N112\text{-}BF_4$ / 0.2 M $Fe(bpy)_3(BF_4)_2$ / MeCN (0.4 M total active species), the electrolyte composition employed later in flow cell experiments, which is 22.5 mS cm^{-1}.

The conductivities of the ionic species increase in the following order: $LiBF_4$ < $Fc1N112\text{-}BF_4$ < $TEABF_4$ < $Fe(bpy)_3(BF_4)_2$. $LiBF_4$ likely exhibits the lowest conductivity because Li^+ is a hard acid and will strongly interact with BF_4^-, a hard base. This interaction leads to a low degree of dissociation and subsequently lower ionic strength in solution for the Li^+ cation salt as compared to the larger and more polarizable TEA^+, $Fc1N112^+$, and $Fe(bpy)_3^{2+}$ cations.[27] $Fe(bpy)_3(BF_4)_2$ exhibits an enhanced conductivity relative to the other salts considered because $Fe(bpy)_3^{2+}$ is a divalent cation, leading to a higher ionic

Author Manuscript

This article is protected by copyright. All rights reserved

strength of the $Fe(bpy)_3(BF_4)_2$ solution as compared to the monovalent cation salts. Since the conductivities of the model ionic active species (Fc1N112-BF_4 and $Fe(bpy)_3(BF_4)_2$) are on the same order of magnitude as $TEABF_4$, a typical supporting salt for NAqRFBs,[1,19,25] they lend themselves for implementation in electrochemical systems without supporting salt.

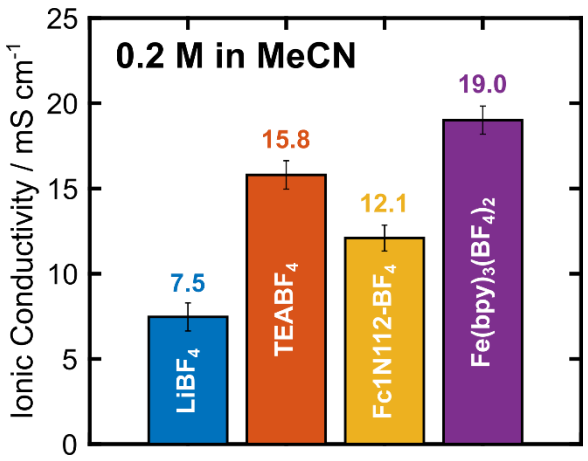

Figure 2. Comparison of electrolyte ionic conductivities for solutions containing 0.2 M of $LiBF_4$, $TEABF_4$, Fc1N112-BF_4, or $Fe(bpy)_3(BF_4)_2$ in MeCN. Error bars represent 95% confidence intervals of the standard error.

Cyclic Voltammetry

Cyclic voltammetry is used to determine if the active species maintain their redox activity in the absence of supporting salt, while further validating that the electrolytes exhibit sufficient ionic conductivity to perform electrochemical measurements. Figure 3 (solid lines) displays CVs of solutions containing the individual active species and an equimolar mixture of each in MeCN, all without supporting salt. The redox potentials and peak height ratios are similar to those of solutions at the same concentration in the presence of supporting salt (Table 1).[15,16,20,24] Notably, the redox potential of Fc1N112-BF_4 is ~70 mV greater than previously reported in a supporting electrolyte of 0.5 M $TBABF_4$ / MeCN. This discrepancy is reconciled when considering that BF_4^- appears in the Nernst equation, resulting in an increase in the equilibrium potential as the supporting salt is removed.

Further analysis of the peak potentials reveals large peak-to-peak separations (Table 1) in the absence of supporting salt, as is anticipated due to the lower solution conductivity with only 5 mM active species in MeCN.[28] To confirm that this large peak-to-peak separation is primarily a result of low solution conductivity and not sluggish reaction kinetics, the CVs are *i*R-corrected (see dashed lines in Figure 3). The uncompensated solution resistance is measured via electrochemical impedance spectroscopy (Figure S3). The *i*R-corrected CVs exhibit significantly smaller peak-to-peak separation values, but are still larger than those for a solution containing 0.5 M tetrabutylammonium tetrafluoroborate[20] ($TBABF_4$) (Table 1). This indicates that the electrokinetics are slightly slower in the regime of low ion concentration, perhaps due to the limited availability of anions. This interpretation is further supported by the decreased peak separation observed with the addition of more active species (i.e., single species vs. the equimolar mixture). These slight differences are expected to have negligible impact during bulk cycling, especially at the high concentrations used in the flow cell experiments. Overall, these results demonstrate that a supporting salt free, one-electron flow cell utilizing Fc1N112-BF_4 and $Fe(bpy)_3(BF_4)_2$ is feasible and should exhibit similar electrochemical behavior to that of a cell containing a high concentration (≥ 0.5 M) of supporting salt.[20]

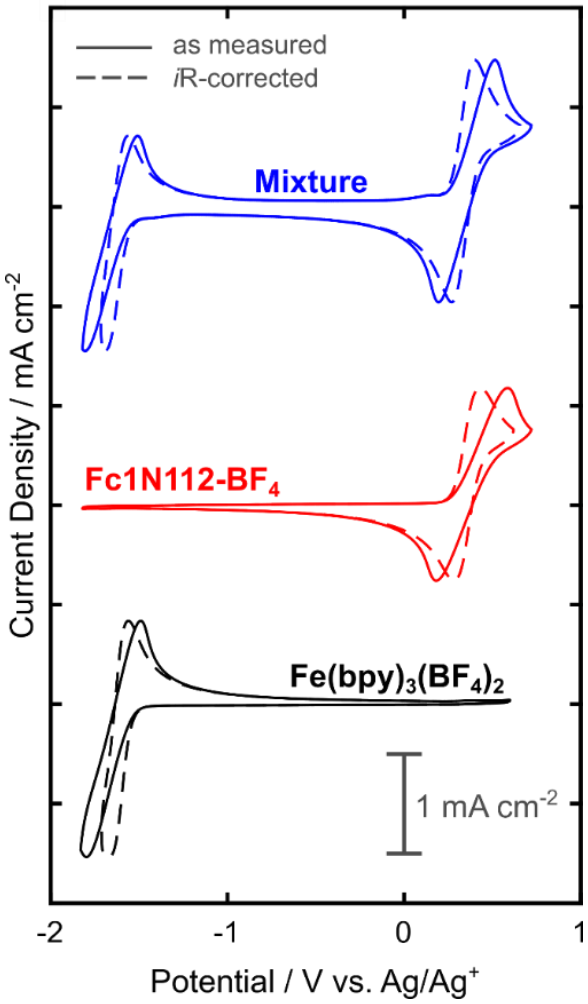

Figure 3. Cyclic voltammograms of 5 mM $Fe(bpy)_3(BF_4)_2$, Fc1N112-BF_4, and an equimolar mixture of each (10 mM total) in MeCN with no supporting salt. For each solution, the solid lines show the data as measured, and the dashed lines represent *i*R-compensated CVs.

Table 1. Comparative CV analysis of electrolytes containing no supporting salt as measured and with *i*R correction, and electrolytes with a supporting salt concentration of 0.5 M $TBABF_4$.[20] In all cases, the active species concentration is 5 mM.

Author Manuscript

This article is protected by copyright. All rights reserved

	5 mM Fc1N112-BF_4			5 mM $Fe(bpy)_3(BF_4)$		
	Potential (V vs. Ag/Ag+)	*Peak Height Ratio*	*Peak Separation (mV)*	*Potential (V vs. Ag/Ag+)*	*Peak Height Ratio*	*Peak Separation (mV)*
No Salt (as measured)	0.35	1.0	405	-1.65	0.9	310
No Salt (*i*R-corrected)	0.36	1.0	147	-1.62	0.9	96
0.5 M $TBABF_4$[20]	0.28	1.0	81	-1.65	0.9	66

Bulk Electrolysis

Bulk electrolysis experiments are used to determine if a cell containing a mixture of $Fe(bpy)_3(BF_4)_2$ and Fc1N112-BF_4 in MeCN (without supporting salt) will access the desired redox couples during cycling. Figure 4 displays capacity retention plots and potential curves for cells cycling through either a single positive or a single negative electron transfer event. In both cases, the plateaus observed during cycling occur at the expected potentials based on CV (Figure 3) and demonstrate that only the desired redox couples are accessed. Furthermore, the results are consistent with those reported in the literature.[15,20] Fc1N112-BF_4 exhibits no detectable capacity fade over the 10 cycles (Figure 4a), which is in agreement with prior reports.[16,20] Not unexpectedly, CVs before and after the bulk electrolysis experiment (Figure S5) show little to no evidence of degradation. Conversely, $Fe(bpy)_3(BF_4)_2$ exhibits capacity decay over the course of the experiment due to the irreversibility of the negative couple.[20] CVs indicate that peak heights associated with the $Fe(bpy)_3^{2+}$ / $Fe(bpy)_3^{+}$ couple decrease after cycling, confirming active species degradation (Figure S5). Despite the suboptimal capacity retention of $Fe(bpy)_3(BF_4)_2$, in both cases the bulk electrolysis cells access the redox couples of interest, confirming the feasibility of using these model active species in a proof-of-concept flow cell without supporting salt.

Author Manuscript

This article is protected by copyright. All rights reserved

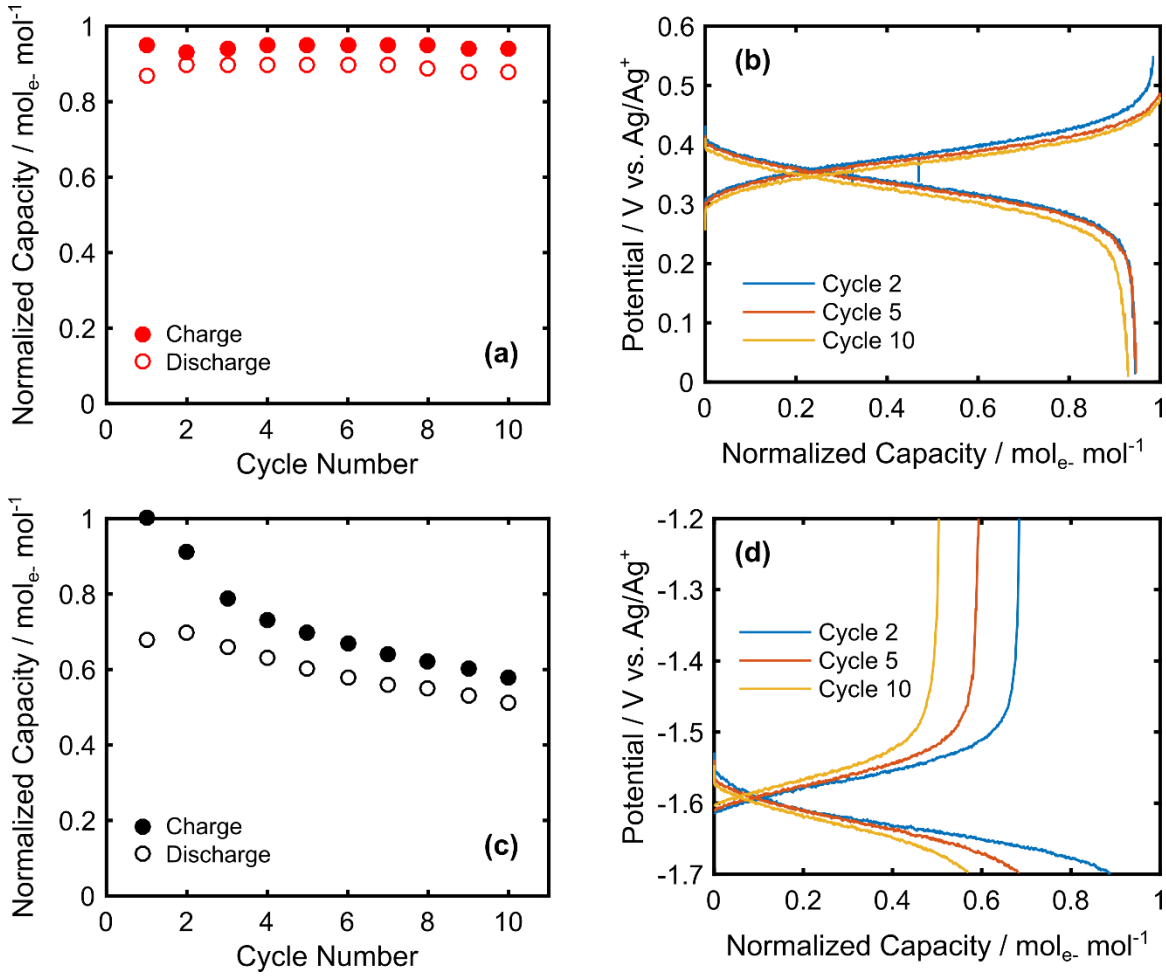

Figure 4. Bulk electrolysis of equimolar mixtures (5 mM each) of $Fe(bpy)_3(BF_4)_2$ and Fc1N112-BF_4 in MeCN, without supporting salt. **(a)** Capacity retention of the mixture, normalized to the theoretical capacity and **(b)** representative charge / discharge curves through a single positive electron transfer. **(c)** Capacity retention, normalized to the theoretical capacity and **(d)** representative charge / discharge curves through a single negative electron transfer.

Author Manuscript

This article is protected by copyright. All rights reserved

Proof-of-Concept Flow Cell

The conductivities and fundamental electrochemical properties of the model ionic active species, $Fe(bpy)_3(BF_4)_2$ and Fc1N112-BF_4, are attractive for incorporation into a proof-of-concept, supporting salt free NAqRFB,. The flow cell has a similar architecture to a high performance all-vanadium flow cell,[29] modified for chemical compatibility with NAq electrolytes.[19,30] Since anion-exchange membranes exhibit limited stability in MeCN,[11,31] Daramic is selected for use as the separator due to its chemical stability in the electrolyte of interest, ensuring that separator degradation would not be a confounding factor in evaluating flow cell performance. Due to the high porosity (58%) and large characteristic pore sizes (~100 nm) for this separator, crossover is expected in these experiments, so both reservoirs are filled with an equimolar mixture of 0.2 M $Fe(bpy)_3(BF_4)_2$ / 0.2 M Fc1N112-BF_4 / MeCN. Prior demonstration studies on RFBs have utilized pre-mixed electrolytes to mitigate effects of rapid crossover in the first few cycles,[20,26,32] although mixed active species electrolytes will be too expensive to implement in grid-scale devices.[6,10] One additional drawback of this configuration is the limited operating concentration of each active species. Adding supporting salt can limit the solubility of active species,[20–22] and similar decreases are observed with the addition of other ionic active species. As a result, an active species concentration of 0.2 M ensures that the species remain soluble at all relevant SOCs.

The flow cell also employs interdigitated flow fields (IDFFs) with carbon paper electrodes. Prior literature has suggested that IDFFs will offer the best performance for large-scale RFBs by balancing cell ASR and pressure drop.[29,33] Additionally, thin carbon paper electrodes offer a balance of high surface area, low ohmic losses, and facile mass transport.[19,34] Despite the relatively thick Daramic separator (175 µm), the cell exhibits an ohmic contribution (R_Ω [Ω cm^2]) to the ASR of just 3.95 Ω cm^2 (Figure 5a) before cycling, a value similar to those reported in a prior flow cell study employing a Daramic separator and MeCN solvent.[25] Combining the IDFF with carbon paper electrodes alleviates mass transfer resistances at each electrode,[19] leading to a flow cell with a total ASR of 7.52 Ω cm^2, determined from an impedance measurement after cycling (Figure 5a, after). Increasing the active species concentration could further reduce mass transfer limitations, as well as improve ionic conductivity, subsequently decreasing the ohmic contribution to the ASR as well.

Further analysis of the impedance spectra reveals that, prior to cycling, the cell exhibits an unbounded, high overall impedance (Figure 5a, before). Since only the fully discharged active species ($Fe(bpy)_3^{2+}$ and $Fc1N112^+$) are present before cycling, the discharge reaction is heavily mass transfer limited and cannot proceed. After cycling, however, residual charged ($Fe(bpy)_3^+$ and $Fc1N112^{2+}$) and discharged species allow for the electrochemical reactions to proceed in either the forward or reverse directions, significantly improving the mass transfer characteristics of the cell at open-circuit voltage (OCV). The bounded semicircle observed after cycling (Figure 5a, after), represents a diffusive mass transfer limitation through a boundary layer of finite thickness.[35] The low-frequency intercept, on the Nyquist plot exhibiting a bounded mass transfer element (Figure 5a, after), represents the total direct current (DC) cell resistance, at a particular SOC, and is typically a good measure of the flow cell ASR.[19,25,30,36]

The relatively low ASR in this study, as compared to those reported for other NAqRFBs,[25,26,37] allows for constant current cycling at a current density of 20 mA cm^{-2}, which is among the highest reported for NAqRFBs.[13,38] Figure 5b illustrates cycling curves of the proof-of-concept supporting salt free NAqRFB, with single charge and discharge plateaus corresponding to the desired one-electron transfer processes and a nominal cell potential of ~1.9 V. To avoid accessing the additional, less stable redox couples of $Fe(bpy)_3(BF_4)_2$ (Figure S4),[20,24] an upper cell potential cutoff of 1.97 V is employed. This cutoff limited the available capacity (Figure 5c) of the first cycle to 32.8% (1.76 Ah L^{-1}) of the theoretical capacity (5.36 Ah L^{-1}). We also limit cycling experiments to 10 cycles due to the known long term instability of $Fe(bpy)_3(BF_4)_2$.[20,24] After the first cycle, the coulombic, voltaic, and energy efficiencies are constant for the remaining 9 cycles, with mean values of 87.3 ± 0.1%, 87.5 ± 0.1%, 76.4 ± 0.1%, respectively (Figure 5d).

Author Manuscript

This article is protected by copyright. All rights reserved

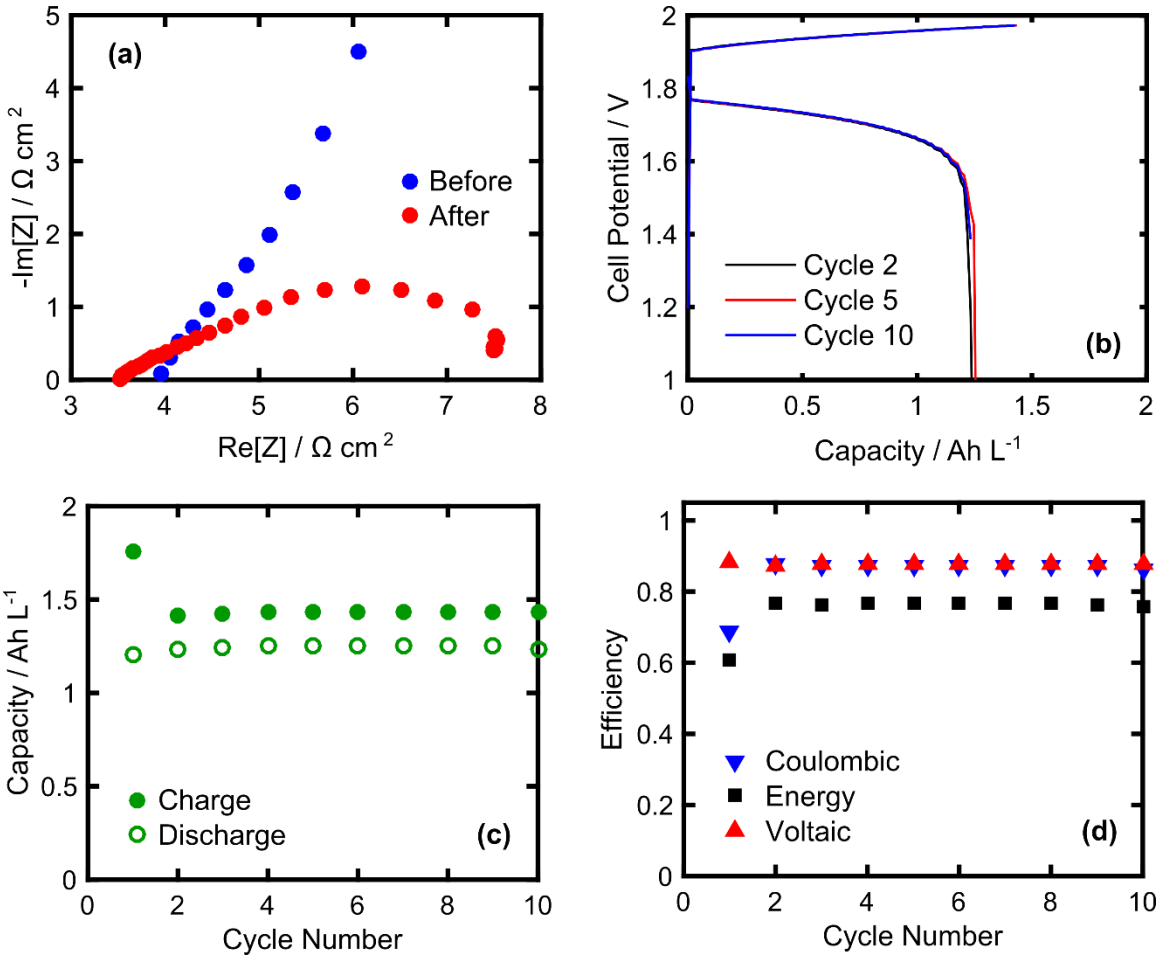

Figure 5. Cycling performance of a supporting salt free NAqRFB employing 0.2 M $Fe(bpy)_3(BF_4)_2$ / 0.2 M Fc1N112-BF_4 / MeCN: **(a)** Nyquist plots before and after 10 cycles, **(b)** representative charge / discharge curves, **(c)** capacities, and **(d)** efficiencies. The theoretical capacity is 5.36 Ah L^{-1} (53.6 mAh), and 10 full cycles completed in ~5.3 h.

Notably, the capacity retention during flow cell cycling is higher than that observed during bulk electrolysis cycling for $Fe(bpy)_3(BF_4)_2$. This result is counterintuitive given the higher concentration of active species employed in the flow cell experiment (0.2 M) as compared to the bulk electrolysis experiment (5 mM) but can be reconciled when considering differences in the accessed capacity. The bulk electrolysis experiments access nearly 100% of the theoretical capacities, as compared to < 33% for the flow cell experiment. Since a smaller fraction of the theoretical capacity is accessed in the flow cell experiment, deleterious side reactions associated with the less stable, reduced $Fe(bpy)_3(BF_4)_2$ species do not degrade the observed capacity as rapidly as in the bulk electrolysis experiment. This phenomena has been reported in prior literature for battery systems with low accessed capacities.[39,40] While the low accessed capacity in this demonstration flow cell is not useful for a grid scale device, the cycling results sufficiently illustrate a proof-of-concept flow cell operating with redox active ions to completely remove the supporting salt.

This proof-of-concept flow cell displays cycling efficiencies similar to state-of-the-art NAqRFBs described in the literature,[25,26] even without any supporting salt. Moderate current density and voltaic efficiencies are achieved because of the high separator conductivity and favorable mass transfer characteristics. The high separator conductivity is achieved by using a microporous separator, in which case the electrolyte conductivity defines the conductivity through the separator pores. Since Daramic is a passive separator, the migration of BF_4^- anions through the separator is sufficiently rapid to afford simultaneously charge balance and moderate currents across the range of accessed SOCs. Critically, the BF_4^- anions act as both charge carriers and charge balancing species in the relevant electrochemical reactions.

To highlight further the dual functionality of the BF_4^- anions, which are associated with the ionic redox active species, we perform a second flow cell cycling experiment where R_Ω is recorded at every half cycle. Figure 6 shows that R_Ω remains nearly constant, oscillating by ± 4.0% about a mean value of

Author Manuscript

This article is protected by copyright. All rights reserved

3.48 Ω cm^2. The small oscillations in R_Ω between half cycles (inset Figure 6), are likely caused by variations in ion-pair association constants as a function of SOC,[30,41] subsequently changing the effective conductivity of the separator and porous electrodes. Oscillations in electrolyte conductivity as a function of SOC are common during RFB cycling, as demonstrated for the all-vanadium RFB[41] and quantified in one NAqRFB electrolyte study.[30] Ultimately, the data in Figure 6 points to a cell devoid of supporting salt that maintains R_Ω values comparable to the contemporary literature.[25]

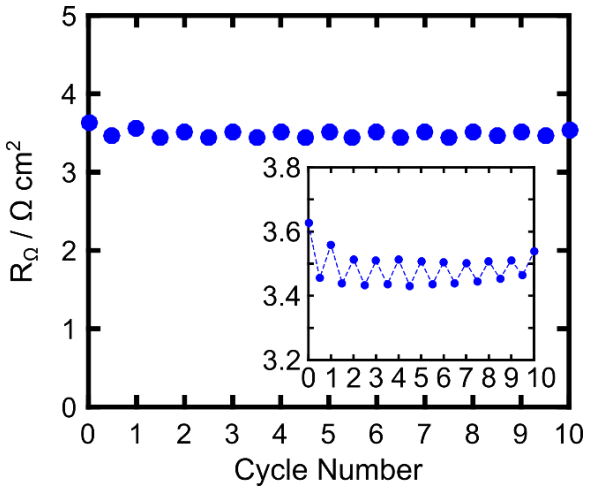

Figure 6. Ohmic contribution to cell ASR measured every half cycle for a supporting salt free NAqRFB. The electrolyte composition is 0.2 M $Fe(bpy)_3(BF_4)_2$ / 0.2 M Fc1N112-BF_4 / MeCN. Inset: Expansion in the R_Ω range of 3.2 – 3.8 Ω cm^2, where the dashed line serves as a visual guide. R_Ω is smaller in the cell's charged state.

Chemistry-Agnostic Techno-Economic Analysis of Salt Free NAqRFBs

To investigate the financial benefits of removing, or minimizing, the supporting salt requirement in NAqRFB electrolytes, we perform a chemistry-agnostic techno-economic analysis to quantify how salt cost and concentration affect battery price. Techno-economic analysis is a powerful tool for evaluating the price performance of an energy storage system by relating the total battery price to material properties, electrochemical performance, and component cost parameters. Given that the proof-of-concept flow cell does not have sufficiently stable or low cost active materials, as well as an insufficient cell potential, we develop a chemistry-agnostic representation that illustrates the cost savings afforded by minimizing supporting salt concentration for a variety of active species costs, salt costs, and cell potentials.

This work employs a prior model developed by Dmello and Milshtein *et al.*,[10] which considers the reactor cost (C_r), electrolyte cost (C_{el}), additional cost (C_{add}), and balance-of-plant (BOP) cost (C_{BOP}) contributions to the battery price per unit energy (P_0 / E_d [\$ kWh^{-1}]), as shown in Equation (4). The reactor cost incorporates the costs of bipolar plates, membranes, and seals, as well as the reactor ASR and battery discharge time. The BOP costs account for auxiliary equipment such as pumps, sensors, tanks, pipes, and heat exchangers, while the additional costs account for overhead, labor, profit margin, and depreciation. Detailed assumptions and calculations of the reactor, additional, and BOP costs are available elsewhere.[6,10] Note that this work considers a future-state battery price, with a 5 h discharge time,[6,8–10] which does not include the cost of installation or power conditioning systems (e.g., inverter), as opposed to a system price that does incorporate such costs.[10] A prior RFB cost modeling study has estimated that installation and power conditioning systems would contribute future-state costs of \$30 kWh^{-1} and \$20 kWh^{-1} (\$100 kW^{-1} over 5 h discharge), respectively, to the RFB system price.[6] Hence, to achieve the DOE system price target of \$150 kWh^{-1},[8,9] we can afford a \$100 kWh^{-1} battery price.[10]

$$\frac{P_0}{E_d} = C_r + C_{el} + C_{add} + C_{BOP} \quad (4)$$

To calculate the electrolyte cost, a detailed model (Equation (5)) explicitly accounts for the costs associated with the electrolyte materials, namely the active species, solvent, and salt.[10] The electrolyte material costs are comprised of the following parameters: M [kg mol^{-1}] is the molar mass of the active species, s is the stoichiometric coefficient of the discharge reaction, χ is the depth-of-discharge, n_e is the number of electrons stored per mole of active material, c_m [\$ kg^{-1}] is the active species cost per unit mass, b [mol kg^{-1}] is the harmonic mean molality of the active species across both electrodes, c_{sol} [\$ kg^{-1}] is the solvent cost per unit mass, M_{salt} [kg mol^{-1}] is the molar mass of the salt, c_{salt} [\$ kg^{-1}] is the salt cost per unit mass, and r_{salt} is the arithmetic mean ratio of moles of salt per mole of active species across both electrodes. The +/– subscripts denote the posolyte and negolyte active materials, respectively. The electrolyte materials costs are normalized by the total discharge energy of the battery, encompassed by the following additional parameters: F [kAh mol^{-1}] is the Faraday constant, and U [V] is the cell potential, while ε_e, ε_q, and ε_v are the energy, coulombic, and voltaic efficiencies, respectively. Here we assume an active species molality of 3 mol kg^{-1}. Assumptions for the values of all other parameters not outlined in this work, are described in detail by Dmello and Milshtein *et al.*[10]

$$C_{el} = \frac{1}{\varepsilon_e \varepsilon_q F \varepsilon_v U}\left(\frac{s_+ M_+}{\chi_+ n_{e+}} c_{m,+} + \frac{s_- M_-}{\chi_- n_{e-}} c_{m,-} + \frac{2}{b} c_{sol} + 2 r_{salt} M_{salt} c_{salt}\right) \quad (5)$$

To illustrate the benefits of reducing salt cost contributions, we define the salt cost factor $\left(C^{\$}_{salt}\right)$ and the active material cost factor $\left(C^{\$}_{m}\right)$ in Equations (6) and (7), respectively, both of which have units of dollars per mole of electrons $\left[\$\ \text{mol}_{e^-}^{-1}\right]$:

$$C^{\$}_{salt} = 2 r_{salt} M_{salt} c_{salt} \quad (6)$$

$$C^{\$}_{m} = \frac{sM}{\chi n_e} c_m \quad (7)$$

Figure 7 shows the relationship between battery price and the salt cost factor for various cell potentials and active material cost factors. In general, as cell potential decreases, the battery price reduces more rapidly with decreasing $\left(C^{\$}_{salt}\right)$, showing that RFB

Author Manuscript

This article is protected by copyright. All rights reserved

price becomes more sensitive to variations in $\left(C^{\$}_{salt}\right)$, at lower cell potentials. Furthermore, battery price rises with increasing $\left(C^{\$}_{salt}\right)$, but variations in $\left(C^{\$}_{m}\right)$ do not affect the slopes of the price curves in Figure 7. Critically, to achieve the recommended battery price of \$100 kWh^{-1},[10] NAqRFBs will require high cell potentials near ~3 V and values of $\left(C^{\$}_{salt}\right)$ near zero,[6,10] the combination of which has yet to be experimentally realized. Decreasing the salt molecular weight (small M_{salt}) or identifying low cost salts (small c_{salt}) are two strategies to decrease $\left(C^{\$}_{salt}\right)$, but considering the prevalence of salts with fluorinated anions in NAqRFB literature, identifying salts with molecular weights lower than that of $LiBF_4$ (93.75 g mol^{-1}) or costs under \$20 kg^{-1}[6] seems unlikely in the near term. In this work, we pursue a third option of minimizing r_{salt}, by removing the salt altogether and setting r_{salt} = 0, which Figure 7 and Equation (5) illustrate is a powerful pathway towards economically viable NAqRFBs.

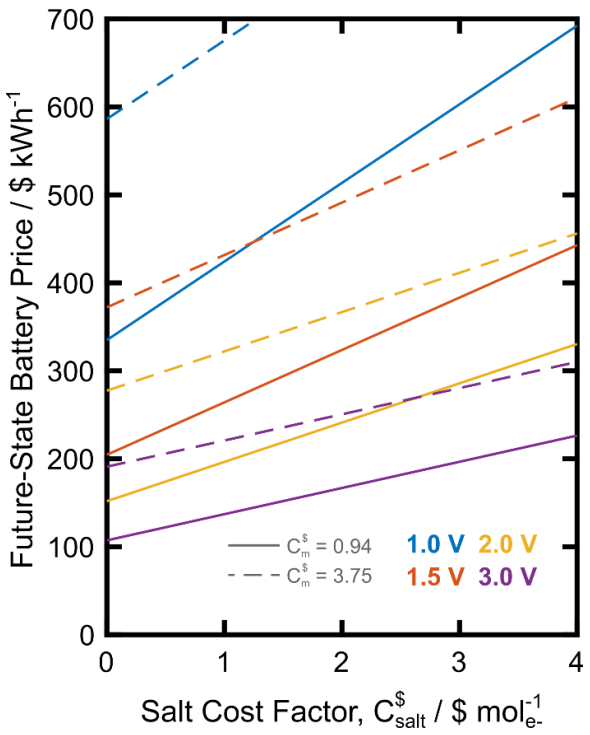

Figure 7. Future-state battery price as a function of salt cost factor $\left(C^{\$}_{salt}\right)$ for various cell potentials (U). Solid lines denote active material cost factors of $C^{\$}_{m} = 0.94$ while dashed lines denote $C^{\$}_{m} = 3.75$. As practical examples, consider a cell with a depth-of-discharge (χ) of 80%, stoichiometric coefficients (s) equal to 1, and active material molecular weight (M) of 150 g mol^{-1}. Then, $C^{\$}_{m} = 0.94$ would represent an active material with a cost (c_m) of \$5 kg^{-1}, and $C^{\$}_{m} = 3.75$ would represent an active material with a cost of \$20 kg^{-1}. Further, $C^{\$}_{salt} = 2$ could represent a salt with molecular weight (M_{salt}) of 100 g mol^{-1} and cost (c_{salt}) of \$20 kg^{-1} dissolved in a ratio of 0.5 moles of salt per mole of active species (r_{salt} = 0.5).

Conclusions

We present a proof-of-concept NAqRFB operating in the absence of supporting salt, utilizing Fc1N112-BF_4 and $Fe(bpy)_3(BF_4)_2$ as model ionic active materials. Efficiencies comparable to state-of-the-art NAqRFBs that employ high concentrations of supporting salt are observed over 10 cycles at a moderate current density (20 mA cm^{-2}). This operation is possible due to the high conductivities of the active species in MeCN, which remain as ions across all relevant SOCs. Solutions of 0.2 M Fc1N112-BF_4 and $Fe(bpy)_3(BF_4)_2$ in MeCN display conductivities of 12.1 and 19.0 mS cm^{-1}, respectively, which is ~2 times higher than the conductivity of 0.2 M $LiBF_4$ and comparable to 0.2 M $TEABF_4$ in the same solvent. Furthermore, a chemistry-agnostic techno-economic analysis highlights the potential cost savings of minimizing salt content in NAqRFBs of varying active material cost, salt cost, and cell potential. Overall, this paper offers proof-of-concept of a NAqRFB operating without supporting salt, opening a pathway for exceptional performance and cost savings.

While the model active species employed in this work are too expensive or unstable for practical grid implementation,[6,10,20,24] our investigation highlights the promise of utilizing ionic redox-active species to enable cost effective NAqRFBs without sacrificing performance. Designing lower-cost counter-anions to replace the existing, expensive fluorinated options (e.g., tetrafluoroborate, hexafluorophosphate) could lead to additional cost savings. Further, ionic modification of otherwise neutral redox active compounds,[15,16] or implementation of deep eutectic, redox active melts[42–44] could be powerful approaches in realizing electrolytes with low salt content. Redox active ionic liquids,[45,46] adapted for flow battery applications, represent an extreme realization of the supporting salt free concept by enabling ultra-high concentration or even solvent free electrolytes. Tailoring ionic active species to display desirable physicochemical (i.e., high solubility[13], low viscosity) and electrochemical properties (i.e., extreme redox potentials[10], stability[13]) will enable the extension of the supporting salt free concept to more practical NAqRFB prototypes.

Experimental Section

Materials

All solution preparation and electrochemical experiments were performed inside argon filled glove boxes (O_2 < 5 ppm, H_2O < 1 ppm). MeCN (Extra Dry, 99.9%) was purchased from Acros Organics. Tetraethylammonium tetrafluoroborate (99.9%) and lithium tetrafluoroborate (99.9%) were purchased from BASF and used as received.

Active Species Synthesis

All reagents and starting materials (iron(II) tetrafluoroborate hexahydrate (97%), (dimethylaminomethyl)ferrocene (96%), bromoethane (98%), sodium tetrafluoroborate (98%)) were purchased from Sigma-Aldrich, with the exception of 2,2'-bipyridine (98%, Alfa Aesar), and used as received. $Fe(bpy)_3(BF_4)_2$ was prepared according to a literature procedure.[20] Fc1N112-BF_4 was synthesized through a bromide salt intermediate also as reported in literature.[15,16,20] Ion exchange of Br^- with BF_4^- was performed in deionized water to afford the final product.[20]

Conductivity Measurements

Author Manuscript

This article is protected by copyright. All rights reserved

Electrolyte conductivity measurements were collected using a two electrode, Swagelok style conductivity cell that has been described previously in literature.[30] The conductivity cell was filled with electrolyte (600 µL) and then sealed. The impedance of the conductivity cell was measured over a small frequency range (1 MHz to 100 Hz) about the OCV with a potential amplitude of 10 mV. The high frequency intercept of the Nyquist plot was used as the cell resistance value for subsequent calculations of electrolyte conductivity. Cell resistances were measured 10 times for 3 aliquots of each electrolyte composition. In between measurements, the conductivity cell was rinsed with pure MeCN. The conductivity cell was calibrated in an ice water bath (0 °C), outside of the glove box, to build a 4-point calibration curve (Figure S2), using the following aqueous sodium chloride standards (Orion™): 0.100, 1.413, 12.90, and 111.9 mS cm^{-1}. NAq electrolyte conductivities were determined from cell resistance measurements and the calibration curve. Error bars for electrolyte conductivities represent 95% confidence intervals of the standard error, accounting for the experimental uncertainties, measurement noise, repeatability, and quality of the calibration fit.

Cyclic Voltammetry

CVs were performed using a BioLogic VSP potentiostat in a custom 10 mL three-electrode electrochemical cell. A 3 mm diameter glassy carbon disk was used as the working electrode (BASi), a coiled platinum wire as the counter electrode, and a fritted Ag/Ag^+ quasi-reference electrode (BASi) filled with silver tetrafluoroborate (0.01 M, 98%, Sigma Aldrich) in MeCN. CVs were recorded at a scan rate of 100 mV s^{-1} in MeCN solutions containing the individual active species (5 mM) or an equimolar mixture containing both $Fe(bpy)_3(BF_4)_2$ and Fc1N112-BF_4 (10 mM total). Impedance measurements were recorded about OCV over a frequency range of 1 MHz to 1 Hz, with a potential amplitude of 10 mV.

Bulk Electrolysis

Bulk electrolysis experiments were performed in a custom glass H-type cell comprised of two electrolyte chambers (5 mL), separated with an ultra-fine glass frit (P5, Adams and Chittenden) to minimize crossover, as described in prior literature.[20] Both chambers were stirred continuously during cycling. Reticulated vitreous carbon (100 PPI, Duocell) was used as the working and counter electrode, with a fritted Ag/Ag^+ quasi-reference electrode. A BioLogic VSP potentiostat was used to apply a constant current equivalent to a C-rate of 1C (0.67 mA). Potential cutoffs (0.55 to 0 V and -1.7 to -1.2 V for the positive and negative experiments, respectively) and a 100% SOC coulombic cutoff were used during cycling. A 3 mm diameter glassy carbon working electrode (BASi) was used to record CVs before and after cycling. For each test, both active species (10 mM total) were dissolved in MeCN.

Flow Cells

The flow cell used in this study is similar to previous literature reports (Figure S6),[19,30] with interdigitated flow fields (IDFFs) and a geometric active area of 2.55 cm^2. Flow cells were assembled outside of the glove box and then dried under vacuum (-91 kPa_g) for at least 1 h before beginning experiments; all electrochemical measurements were performed inside the glovebox. Backing plates were machined from polypropylene, and flow fields were machined from 3.18 mm thick impregnated graphite (G347B graphite, MWI, Inc.). Electrodes were cut (16.1 mm × 14.1 mm) from 190 ± 30 µm thick carbon paper (25 AA, SGL Group) and used as received, without any pre-treatment. Carbon paper electrodes were layered two pieces thick and compressed by 20 ± 2% in the assembled flow cell, yielding a final total compressed electrode thickness of 304 ± 49 µm. A single layer of Daramic 175 was used as received as the cell separator. Teflon gaskets sealed the separator and electrodes inside the cell. Sealed jars (10 mL, Savillex), made from perfluoroalkoxy alkane (PFA), served as the electrolyte reservoirs. A peristaltic pump (Masterflex L/S Series) was used to drive electrolyte through the flow cell and reservoirs. Norprene tubing (Masterflex) was used inside the peristaltic pump head. PFA tubing (Swagelok) linked together the pump head, flow cell, and reservoirs. All tubing connections were made with pressure rated PFA (Swagelok), Teflon (Swagelok), or stainless steel (McMaster-Carr) compression fittings. Further, all tubing had an inner diameter of 1.6 mm (Figure S7). All flow cell materials (polypropylene, impregnated graphite, PFA, Teflon, stainless steel, and Daramic) were selected in part due to their chemical compatibility with MeCN.

Pre-mixed electrolyte (10 mL), containing $Fe(bpy)_3(BF4)_2$ (0.2 M) / Fc1N112-BF_4 (0.2 M) / MeCN, was pumped into each flow cell reservoir. For the redox couples accessed, the theoretical capacity of the electrolyte was 5.36 Ah L^{-1} (53.6 mAh). During the first flow cell cycling experiment, a constant current density of 20 mA cm^{-2} (51 mA) was applied, and cell potential cutoffs of 1.00 – 1.97 V were imposed. The upper voltage cutoff was selected to avoid accessing additional, unstable redox couples of $Fe(bpy)_3(BF_4)_2$, and the lower voltage cutoff ensured complete discharge of the cell. The cell was cycled 10 times over ~5.3 h. Flow cell impedance measurements before and after the first flow cell experiment were recorded about OCV over a frequency range of 100 kHz to 5 mHz, with a potential amplitude of 10 mV. A second flow cell cycling experiment was performed in which constant current cycling (20 mA cm^{-2}) was paused at each half cycle to measure flow cell impedance in a higher frequency regime (100 kHz to 20 Hz).

Acknowledgements

J. D. M. and S. L. F. contributed equally to this work. This project was supported by the Joint Center for Energy Storage Research (JCESR), an Energy Innovation Hub funded by the United States Department of Energy. J. D. M. and S. L. F. acknowledge the National Science Foundation Graduate Research Fellowship Program for additional funding. We thank Dr. Kyle Smith and Rylan Dmello from the University of Illinois at Urbana-Champaign for their assistance developing the MATLAB code used to perform the techno-economic analysis. We also thank other members of the JCESR Flow Chemistry team, including Dr. Xiaoliang Wei, Dr. Rama Vemuri, Dr. Wentao Duan, Dr. Robert Darling, Dr. Krista Hawthorne, and Vinay Iyer. Finally, we appreciate the valuable feedback from members of the Thompson Group at the University of Michigan and the Brushett Group at the Massachusetts Institute of Technology throughout the project.

Keywords: energy storage • electrochemistry • non-aqueous flow battery • redox chemistry • techno-economic analysis

[1] W. Wang, Q. Luo, B. Li, X. Wei, L. Li, Z. Yang, *Adv. Funct. Mater.* **2013**, *23*, 970–986.

[2] A. Z. Weber, M. M. Mench, J. P. Meyers, P. N. Ross, J. T. Gostick, Q. Liu, *J. Appl. Electrochem.* **2011**, *41*, 1137–1164.

[3] M. Skyllas-Kazacos, M. H. Chakrabarti, S. A. Hajimolana, F. S. Mjalli, M. Saleem, *J. Electrochem. Soc.* **2011**, *158*, R55–R79.

Author Manuscript

This article is protected by copyright. All rights reserved

[4] P. Denholm, E. Ela, B. Kirby, M. Milligan, *The Role of Energy Storage with Renewable Electricity Generation: NREL/TP-6A2-47187*, **2010**.

[5] B. Dunn, H. Kamath, J. M. Tarascon, *Science (80-.).* **2011**, *334*, 928–935.

[6] R. M. Darling, K. G. Gallagher, J. A. Kowalski, S. Ha, F. R. Brushett, *Energy Environ. Sci.* **2014**, *7*, 3459–3477.

[7] V. Viswanathan, A. Crawford, D. Stephenson, S. Kim, W. Wang, B. Li, G. Coffey, E. Thomsen, G. Graff, P. Balducci, et al., *J. Power Sources* **2014**, *247*, 1040–1051.

[8] D. Rastler, *Market Driven Distributed Energy Storage Requirements for Load Management Applications*, Palo Alto, CA, **2007**.

[9] U.S. Department of Energy: Office of Electricity Delivery and Energy Reliability, *Energy Storage: Program Planning Document*, **2011**.

[10] R. D. Dmello, J. D. Milshtein, F. R. Brushett, K. C. Smith, *J. Power Sources* **2016**, *330*, 261–272.

[11] S. H. Shin, S. H. Yun, S. H. Moon, *RSC Adv.* **2013**, *3*, 9095–9116.

[12] W. Wang, V. Sprenkle, *Nat. Chem.* **2016**, *8*, 204–206.

[13] J. A. Kowalski, L. Su, J. D. Milshtein, F. R. Brushett, *Curr. Opin. Chem. Eng.* **2016**, *13*, 45–52.

[14] J. Huang, L. Cheng, R. S. Assary, P. Wang, Z. Xue, A. K. Burrell, L. A. Curtiss, L. Zhang, *Adv. Energy Mater.* **2015**, *5*, 1401782.

[15] L. Cosimbescu, X. Wei, M. Vijayakumar, W. Xu, M. L. Helm, S. D. Burton, C. M. Sorensen, J. Liu, V. Sprenkle, W. Wang, *Sci. Rep.* **2015**, *5*, 14117.

[16] X. Wei, L. Cosimbescu, W. Xu, J. Z. Hu, M. Vijayakumar, J. Feng, M. Y. Hu, X. Deng, J. Xiao, J. Liu, et al., *Adv. Energy Mater.* **2014**, *5*, 1400678.

[17] P. J. Cabrera, X. Yang, J. A. Suttil, K. L. Hawthorne, R. E. M. Brooner, M. S. Sanford, L. T. Thompson, *J. Phys. Chem. C* **2015**, *119*, 15882–15889.

[18] P. J. Cabrera, X. Yang, J. A. Suttil, R. E. M. Brooner, L. T. Thompson, M. S. Sanford, *Inorg. Chem.* **2015**, *54*, 10214–10223.

[19] J. D. Milshtein, A. P. Kaur, M. D. Casselman, J. A. Kowalski, S. Modekrutti, P. Zhang, N. H. Attanayake, C. F. Elliott, S. R. Parkin, C. Risko, et al., *Energy Environ. Sci.* **2016**, DOI 10.1039/C6EE02027E.

[20] S. M. Laramie, J. D. Milshtein, T. M. Breault, F. R. Brushett, L. T. Thompson, *J. Power Sources* **2016**, *327*, 681–692.

[21] A. A. Shinkle, T. J. Pomaville, A. E. S. Sleightholme, L. T. Thompson, C. W. Monroe, *J. Power Sources* **2014**, *248*, 1299–1305.

[22] J. R. Dahn, J. Jiang, L. M. Moshurchak, M. D. Fleischauer, C. Buhrmester, L. J. Krause, *J. Electrochem. Soc.* **2005**, *152*, A1283–A1289.

[23] L. Su, R. M. Darling, K. G. Gallagher, W. Xie, J. L. Thelen, A. F. Badel, J. L. Barton, K. J. Cheng, N. P. Balsara, J. S. Moore, et al., *J. Electrochem. Soc.* **2016**, *163*, A5253–A5262.

[24] M. H. Chakrabarti, R. A. W. Dryfe, E. P. L. Roberts, *Electrochim. Acta* **2007**, *52*, 2189–2195.

[25] I. Escalante-Garcia, J. S. Wainright, L. T. Thompson, R. F. Savinell, *J. Electrochem. Soc.* **2015**, *162*, A363–A372.

[26] X. Wei, W. Xu, J. Huang, L. Zhang, E. Walter, C. Lawrence, M. Vijayakumar, W. A. Henderson, T. Liu, L. Cosimbescu, et al., *Angew. Chemie Int. Ed.* **2015**, *54*, 8684–8687.

[27] M. Ue, *J. Electrochem. Soc.* **1994**, *141*, 3336.

[28] S. R. Belding, R. G. Compton, *J. Electroanal. Chem.* **2012**, *683*, 1–13.

[29] R. M. Darling, M. L. Perry, *J. Electrochem. Soc.* **2014**, *161*, A1381–A1387.

[30] J. D. Milshtein, J. L. Barton, R. M. Darling, F. R. Brushett, *J. Power Sources* **2016**, *327*, 151–159.

[31] N. S. Hudak, L. J. Small, H. D. Pratt, T. M. Anderson, *J. Electrochem. Soc.* **2015**, *162*, A2188–A2194.

[32] Y. K. Zeng, X. L. Zhou, L. An, L. Wei, T. S. Zhao, *J. Power Sources* **2016**, *324*, 738–744.

[33] C. R. Dennison, E. Agar, B. Akuzum, E. C. Kumbur, *J. Electrochem. Soc.* **2015**, *163*, A5163–A5169.

[34] Q. H. Liu, G. M. Grim, a. B. Papandrew, A. Turhan, T. A. Zawodzinski, M. M. Mench, *J. Electrochem. Soc.* **2012**, *159*, A1246–A1252.

[35] X.-Z. Yuan, C. Song, H. Wang, J. Zhang, *Fundam. Appl. London* **2010**.

[36] C.-N. Sun, F. M. Delnick, D. S. Aaron, A. B. Papandrew, M. M. Mench, T. A. Zawodzinski, *J. Electrochem. Soc.* **2014**, *161*, A981–A988.

[37] M. Park, N. Lee, S. Lee, K. J. Kim, D. Oh, Y. Kim, *ACS Appl. Mater. Interfaces* **2014**, *6*, 10729–10735.

[38] W. Duan, R. S. Vemuri, J. D. Milshtein, S. Laramie, R. D. Dmello, J. Huang, L. Zhang, D. Hu, M. Vijayakumar, W. Wang, et al., *J. Mater. Chem. A* **2016**, *4*, 5448–5456.

[39] A. J. Smith, J. C. Burns, D. Xiong, J. R. Dahn, *J. Electrochem. Soc.* **2011**, *158*, A1136.

[40] A. Orita, M. G. Verde, M. Sakai, Y. S. Meng, *J. Power Sources* **2016**, *321*, 126–134.

[41] M. Skyllas-Kazacos, M. Kazacos, *J. Power Sources* **2011**, *196*, 8822–8827.

[42] M. A. Miller, J. S. Wainright, R. F. Savinell, *J. Electrochem. Soc.* **2016**, *163*, A578–A579.

[43] L. Bahadori, M. A. Hashim, N. S. A. Manan, F. S. Mjalli, I. M. AlNashef, N. P. Brandon, M. H. Chakrabarti, *J. Electrochem. Soc.* **2016**, *163*, A632–A638.

[44] M. H. Chakrabarti, F. S. Mjalli, I. M. AlNashef, M. A. Hashim, M. A. Hussain, L. Bahadori, C. T. J. Low, *Renew. Sustain. Energy Rev.* **2014**, *30*, 254–270.

[45] E. Mourad, L. Coustan, S. A. Freunberger, A. Mehdi, A. Vioux, F. Favier, O. Fontaine, *Electrochim. Acta* **2016**, *206*, 3–8.

[46] J. Park, M. Lee, S. Hwang, D. Lee, D. Oh, *Redox Flow Battery: US2012/0171541 A1*, **2012**.

Author Manuscript

This article is protected by copyright. All rights reserved

FULL PAPER

Decreasing salt cost contribution to the total electrolyte cost for non-aqueous redox flow batteries is essential for economic viability. We demonstrate a non-aqueous flow battery utilizing all-ionic active materials that completely removes the need for a supporting salt. The cell cycling performance and area-specific specific resistance are comparable to state-of-the-art non-aqueous flow cells employing high concentrations of salt.

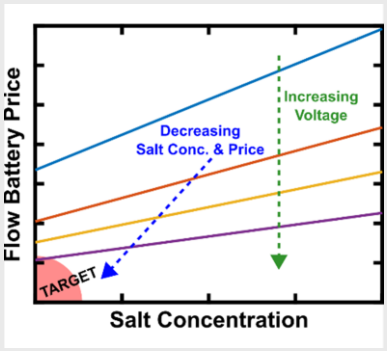

Jarrod D. Milshtein,[§] Sydney L. Fisher,[§] Tanya M. Breault, Levi T. Thompson, Fikile R. Brushett**

Page No. – Page No.

Feasibility of a supporting salt free non-aqueous redox flow battery utilizing ionic active materials

Author Manuscript

This article is protected by copyright. All rights reserved